Welding in the World (2023) 67:513–524
https://doi.org/10.1007/s40194-022-01448-5

RESEARCH PAPER

# Microstructure, mechanical properties and corrosion behaviour of Ti6Al4V/$Al_2O_3$ joints brazed with TiCuNi filler

A. C. Alves[1,2,3] · A. M. P. Pinto[1,2,4] · S. Simões[5,6] · A. Guedes[1,2,4]

Received: 5 April 2022 / Accepted: 11 December 2022 / Published online: 21 December 2022


## Abstract

Ti6Al4V and $Al_2O_3$ were successfully vacuum brazed at 980 °C using TiCuNi filler foil. The microstructure and the chemical composition of the interface were analysed by SEM (scanning electron microscopy) and EDS (energy dispersive spectroscopy), respectively. The hardness profile across the interface and the mechanical strength of joints were assessed by Vickers microhardness tests and shear tests, respectively. The fracture surfaces were analysed by SEM, EDS and XRD (X-ray diffraction). The corrosion behaviour of joints was evaluated by OCP (open circuit potential), potentiodynamic polarisation tests and EIS (electrochemical impedance spectroscopy). Brazing produced a layered interface, free of pores and cracks, essentially composed of α-Ti, $Ti_2$(Cu,Ni) and $Ti_xO_y$. The shear strength of joints was 168 ± 13 MPa, and fracture occurred partially through the hardest zone of the interface (1261 $HV_{0.01}$.), located in the vicinity of the $Al_2O_3$ sample, and partially through the ceramic sample. The brazed joint did not significantly affect the corrosion behaviour of Ti6Al4V.

**Keywords** Ti6Al4V · $Al_2O_3$ · Brazing · Mechanical properties · Corrosion

## 1 Introduction

$Al_2O_3$ is an appealing material for applications related to nuclear, aerospace or automotive industries due to its high specific mechanical strength, thermal and chemical stability, high hardness and wear resistance [1, 2]. However, $Al_2O_3$ brittleness and low ductility lead to poor processing performance, limiting its use in complex structures [2]. Therefore, to overcome these drawbacks, $Al_2O_3$ is often required to be joined to metallic materials such as Ti alloys, which combine good mechanical properties and excellent processability. Ti6Al4V is known for its high performance in aerospace or chemical industries due to its high specific strength, relatively high thermal stability and excellent corrosion resistance [3, 4]. Adequate Ti6Al4V/$Al_2O_3$ joints allow taking advantage of the distinct properties of both materials in multi-material components.

Vacuum brazing [2, 5] and active metal brazing [6, 7] are well reported to be appropriate techniques to join $Al_2O_3$ to Ti-based alloys and to other metals. When joining Ti6Al4V, it is imperative not to exceed the β-transus temperature (c.a. 995 °C), since once that temperature threshold is crossed, the fine equiaxial microstructure is lost and the characteristics mechanical properties of Ti6Al4V are jeopardised [8, 9]. TiCuNi is a clad-laminated brazing filler known

Recommended for publication by Commission XVII - Brazing, Soldering and Diffusion Bonding

✉ A. C. Alves
alexandra@dem.uminho.pt

1 CMEMS-UMinho – Center of MicroElectroMechanical Systems, Universidade do Minho, Campus de Azurém, 4800-058 Guimarães, Portugal

2 LABBELS – Associate Laboratory, Braga, Guimarães, Portugal

3 IBTN/Euro – European Branch of the Institute of Biomaterials, Tribocorrosion and Nanomedicine, Dept. Eng. Mecânica, Universidade do Minho, Azurém, 4800-058 Guimarães, Portugal

4 DEM-UMinho – Department of Mechanical Engineering, University of Minho, Campus de Azurém, 4800-058 Guimarães, Portugal

5 DEMM – Department of Metallurgical and Materials Engineering, Faculdade de Engenharia da Universidade do Porto, Porto, Portugal

6 LAETA/INEGI, Institute of Science and Innovation in Mechanical and Industrial Engineering, R. Dr. Roberto Frias, 4200-465 Porto, Portugal

to successfully braze Ti and Ti Alloys [10, 11]. Contrarily to Ag–Cu eutectic-based brazing alloys, TiCuNi does not induce the formation of (Ag) at the interfaces, which strongly limits the maximum operating temperature of joints [12]. However, TiCuNi filler induces an extensive formation of presumably brittle intermetallics at the interface, which couple with the lack of ductile phases such (Ag), should have a detrimental effect on the room temperature performance of the joints, in comparison to the use of Ag–Cu eutectic-based brazing fillers.

It is well reported that the brazing interface is the most critical region of joints since the reaction products formed at the interface are the main factor determining the mechanical performance and the corrosion behaviour of joints. However, studies on the corrosion behaviour of brazed Ti6Al4V/$Al_2O_3$ joints are scarce, and to the best of our knowledge, there are no reports on the subject regarding the use of TiCuNi as brazing filler. Some of the present authors used TiCuNi to join cp Ti [13] and Ti-$B_4C$ composites [14], reporting no adverse effect on the corrosion behaviour of joints and showing the promising use of TiCuNi as a brazing alloy. The present work focuses on the effect of TiCuNi braze alloy on the microstructural features of the interface and on the mechanical strength and corrosion behaviour of Ti6Al4V/$Al_2O_3$ joints.

## 2 Materials and methods

Ti6Al4V (∅ – 10 mm) and $Al_2O_3$ (∅ – 6 mm, 99% purity) samples, both from Goodfellow. The shear strength of the ceramic is 330 MPa, and its Vickers hardness ranges from 1500 to 1650 (kgf $mm^{-2}$). The base materials were cut with a diamond disk to 10-mm height samples and ground down to #600 SiC paper finish. Prior to brazing, all materials were ultrasonically cleaned for 10 min in isopropyl alcohol, followed by 5 min in distilled water. Ti6Al4V/$Al_2O_3$ joints for microstructural and chemical characterisation of the interface, as well as for shear tests and for electrochemical tests, were produced by vacuum brazing using a 90-μm-thick TiCuNi (Ti – 15Cu – 15Ni, wt.%, from Morgan Advanced Materials) filler foil that presents a liquidus temperature of 960 °C. The Ti6Al4V/TiCuNi/$Al_2O_3$ assemblage was carefully positioned into a stainless steel fixing apparatus and brazed in a high vacuum furnace (vacuum level better than $10^{-5}$ mbar). Brazing was performed at 980 °C, which was the minimum temperature below β-transus, at which sound interfaces could be produced. The dwelling stage at the brazing temperature was of 10 min, and the heating and cooling rates were set to 5 °C/min.

Cross-sections of the brazed joints were obtained by cutting the brazed samples perpendicularly to the interface with a diamond disk. For electrochemical tests, the brazed cross-sectional surfaces were ground down #1200 SiC papers, while for microstructural characterisation of the interface, mirror finish surfaces were prepared using standard metallographic procedures. Afterwards, the samples were ultrasonically cleaned using the same procedure previously described. The microstructure and chemical composition of the as-brazed and of the corroded interfaces, as well as of the fracture surfaces and of the cross-sections of shear-tested joints, were analysed using an FEI (Oregon, USA) Nova 200 scanning electron microscope (FEG/SEM) with an EDAX—Pegasus X4 M integrated EDS system. Unless otherwise stated, hereafter, all compositions will be expressed in at.%.

Shear testing of joints was carried out at room temperature, in a universal testing machine (Instron 8874, MA, USA), with a 25-kN load cell using under a crosshead speed of 0.5 mm/min. Tests were performed using a custom-made stainless steel set-up (Fig. 1). A total of 9 Ti6Al4V/$Al_2O_3$ joints were tested. Phases detected on the fracture surface of joints were identified by X-ray diffraction (XRD) with a Bruker D8 Discover diffractometer using Cu Kα radiation.

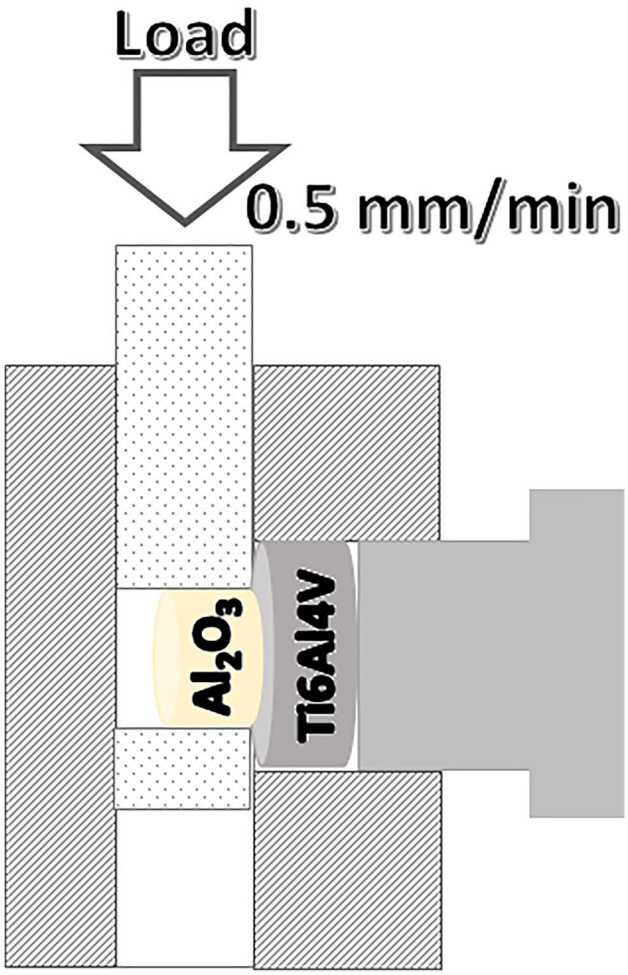


**Fig. 1** Schematic representation of the shear test set-up

The hardness profile and the hardness distribution map across the interface were assessed by Vickers microhardness tests using Emcotest Durascan Microhardness tester, under 0.01 kgf during 15 s. Each point on the hardness profile corresponds to the average hardness value of at least 5 indentations performed on similar zones of the interface. A typical indentation matrix consisted of 4 rows by 7 columns. The spacings between each consecutive row and column were 25 µm and 35 µm, respectively.

The corrosion tests were performed using 3.5%wt. of aqueous NaCl solution at room temperature immediately after metallographic preparation. A typical three-electrode set-up of an electrochemical cell (adapted from ASTM: G3-89) was used in the electrochemical tests, where the brazed joints and Ti6Al4V samples were plugged as working electrode (having 0.1 $cm^2$ of exposed area), the counter electrode was a Pt net, and saturated Ag/AgCl was used as the reference electrode. Lastly, all the electrodes were plugged to a Gamry Potentiostat/Galvanostat/ZRA (reference—$600^+$). Considering that the $Al_2O_3$ part of brazed joints does not contribute for the corrosion mechanism of the joints, the exposed area was considered to be just the metallic part (0.05 $cm^2$). The electrochemical parameters of the joints were normalised by this area.

The electrochemical tests consisted in sequential order of open circuit potential (OCP), electrochemical impedance spectroscopy (EIS) and finally potentiodynamic polarisation tests. OCP was monitored until the stabilisation of the system, which was considered stable when $\Delta E < 60$ mV/h. EIS measurements were performed at OCP by scanning within a frequency range from $10^5$ to $10^{-2}$ Hz, with 7 points per decade. The linearity of the electrode response was guaranteed with 10 mV of the sinusoidal signal. Gamry Echem Analyst software was used to fit the experimental EIS data. The quality of the proposed electrical equivalent circuit (EEC) and its goodness of fitting ($\chi^2$) was used to determine the EEC fitting quality. Finally, the potentiodynamic polarisation tests were executed by scanning a potential range in the anodic direction with 0.5 mV/s starting from $-0.25$ $V_{OCP}$ up to 2.0 $V_{Ag/AgCl}$.

In order to understand the evolution of the $R_p$ (polarisation resistance) with different immersion periods, linear polarisation scans were performed after 24 h, 48 h, 96 h (4 days) and 192 h (8 days) of immersion at $\pm 20$ $mV_{OCP}$ using a scanning rate of 0.5 mV/s. $R_p$ was extracted from linear polarisation tests by using Gamry Echem Analyst software version 7.1.

## 3 Results and discussion

Figure 2 displays SEM images of the interface. TiCuNi filler reacted with both base materials promoting the formation of a layered interface. The interface is c.a. 130 µm thick with no perceived porosity, cracks and zones lacking bonding. No alterations of either on the composition and on the microstructure of the base materials were detected after joining. The interface could be divided into two main layers (labelled as A and B in Fig. 2), both extending from the centre of the interface, one into Ti6Al4V (layer A) and the other into $Al_2O_3$ (layer B). The information from the isothermal section of the Ti-Cu-Ni equilibrium phase diagram [15] and SEM images presented in Fig. 2, along with EDS analysis results (Table 1), were used together to predict the nature of the phases formed at the interface. Furthermore, Cu and Ni will be considered to behave in a similar manner, as Lee et al. [16, 17] did, since Cu and Ni atoms have similar atomic sizes and electronegativities, and in addition, Cu and Ni present the same crystal structure and total solubility in the solid state. Therefore, $Ti_xCu$ and $Ti_xNi$ intermetallics will be referred to as $Ti_x(Cu,Ni)$.

Layer A is composed of a mixture of coarse grey particles and lamellar zones (Z1 and Z2, respectively, in Fig. 2). The coarse grey particles were mainly detected near Ti6Al4V and composed of more than 80% Ti, and thus, it should consist of α-Ti with Cu and Ni contents not exceeding 2%. The plot of the chemical composition of the lamellar zones lies on the ($Ti_2(Cu,Ni)$ + α-Ti) two-phase field, closer to α-Ti single-phase domain. Therefore, the lamellar zones should consist of α-Ti and $Ti_2(Cu,Ni)$ lamellae, with the predominance of α-Ti.

Layer B consists of coarse white particles (Z3), mixed with lamellar zones and grey particles. In addition, close to $Al_2O_3$, Ti–Al-Ni–O rich particles (Z4), forming a discontinuous sub-layer, presumably consisting of oxide phase(s), were also observed. It should be noted that these particles are quite thin, and consequently, the volume interaction on the EDS analysis of the zones around and below them may lead to misleading results. For instance, a Ti-Cu-Ni-rich phase surrounds these particles, and in addition, they are detected in the close vicinity of the base $Al_2O_3$. However, these particles are the only zones of the interface where oxygen is detected in substantial amounts by EDS analysis. The chemical composition of the coarse white particles is located close to both $Ti_2Cu$ single-phase field and ($Ti_2Cu + Ti_2Ni$) two-phase field, which are depicted as adjacent elongated narrow phase fields on the ternary phase diagram presented in Fig. 2. Considering that Cu and Ni atoms may substitute each other due to their similar characteristics, the coarse white particles should consist of $Ti_2(Cu,Ni)$. It should be noted that these particles were also sporadically observed in layer A. Finally, the grey particles and the lamellar zones in layer B present almost the same composition as the related zones/particles in layer A and should consist of the same phases.

The proposed nature of phases formed at the interface is consistent with the phases described in other studies. For example, the lamellar constituent as a mixture of α-Ti and $Ti_2(Cu,Ni)$ has been

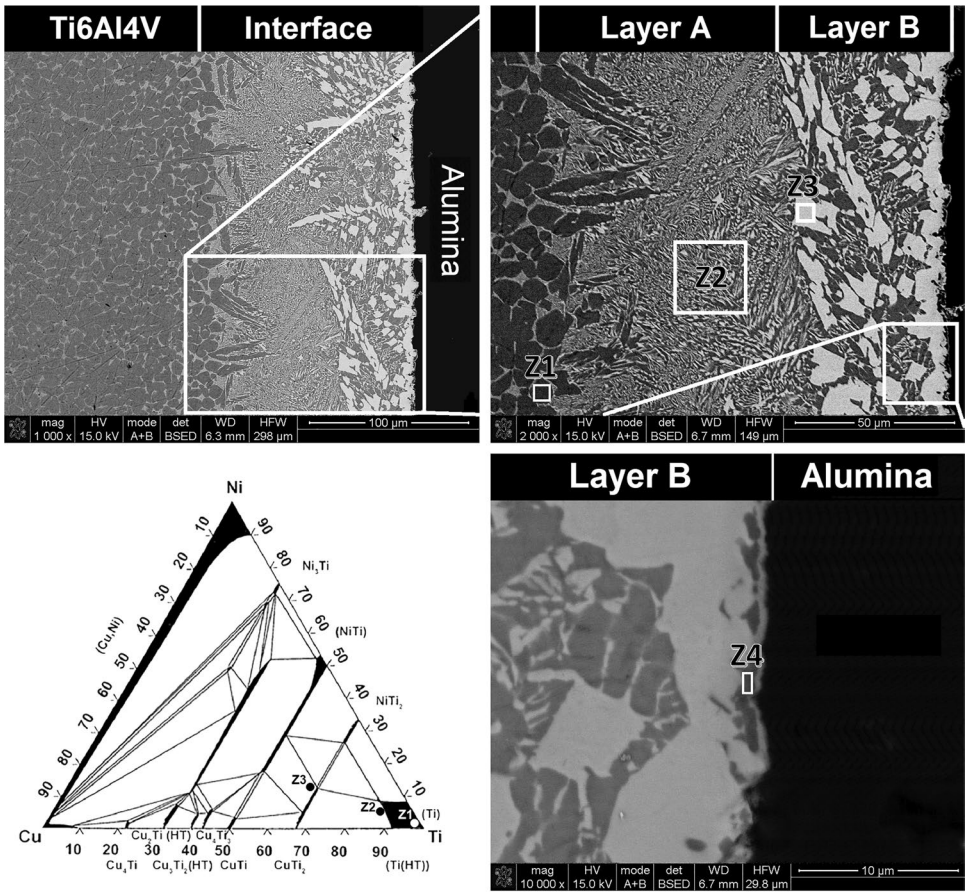


**Fig. 2** SEM images of Ti6Al4V/TiCuNi/$Al_2O_3$ brazed joints, showing a global view and detailed microstructural features of the interface, together with the isothermal section at 800 °C of TiCuNi phase diagram, which was adapted from [15]

**Table 1** Chemical composition of zones shown in Fig. 2

| Zones | Chemical composition (at.%) | | | | | | Possible phase |
|---|---|---|---|---|---|---|---|
| | Ti | Al | V | Cu | Ni | O | |
| Z1 | 84.2 | 11.6 | 0.9 | 2.0 | 1.3 | – | αTi |
| Z2 | 80.2 | 6.8 | 1.0 | 6.1 | 5.9 | – | αTi + $Ti_2$(Cu,Ni) |
| Z3 | 65.3 | 1.3 | 0.1 | 22.2 | 11.1 | – | $Ti_2$(Cu,Ni) |
| Z4 | 36.8 | 24.4 | – | 3.4 | 2.2 | 33.2 | Oxide(s) |

reported by several authors on the joining of Ti-based materials using TiCuNi as a filler alloy. Marinho et al. [13] joined c.p. Ti using TiCuNi as filler and specified that the interface was composed of two distinct layers: a central zone and a diffusion layer that extended to the base material. The central zone was characterised as a lamellar constituent consisting of a mixture of α-Ti and $Ti_2$(Cu,Ni) intermetallics. On the other hand, Sousa et al. [14] used the same filler to join Ti-$B_4C$ composites and reported α-Ti + $Ti_2$(Cu,Ni) lamellar constituent at the central zone of the interface. It should also be noted that studies on the joining of Ti6Al4V using TiCuNi as filler alloy reported the formation of a Widmanstätten structure where $Ti_2$(Cu,Ni) particles were delimiting α-Ti plates [18–20]. It is reported that β-transus temperature of Ti6Al4V might be reduced by the diffusion of Cu and Ni elements during the brazing thermal cycle. Consequently, in the course of the joining, the α-Ti matrix with diffused Cu and Ni transforms into β-Ti. However, during cooling, the β phase converts again into α phase and leads to the formation of the acicular Widmanstätten structure [18]. Some of the coarse grey particles detected in layer A present a plate-like shape and are mostly surrounded by a white phase, which should be $Ti_2$(Cu,Ni). Therefore, a similar formation mechanism to the aforementioned may be envisaged for the grey particles observed in layer A. Finally, regarding the possible formation of oxide phases close to $Al_2O_3$, eventually Ti oxides and/or mixed Ti–Al oxides, it should be noted that these are reported to be responsible for the establishment of a successful joint, once they promote chemical bonding between the metallic and ceramic phases constituting the interface [21].

The interfacial hardness profile and the interfacial hardness distribution map of joints are presented in Fig. 3. The interface is harder than the

base Ti6Al4V alloy (c.a. 398 $HV_{0.01}$), and the general trend of the profile is the increment in hardness from the metal side towards the ceramic side of the interface. The hardness of layer A varies between around 450 and 500 $HV_{0.01}$, while the hardness of the lamellar zones and the hardness of the coarse white phase, probably composed of $Ti_2$(Cu,Ni), remain roughly unchanged across the interface, typically around 475 $HV_{0.01}$ and 525 $HV_{0.01}$, respectively. It should be noted that these hardness values are in good agreement with those reported by Eroglu et al. [22] that joined Ti6Al4V to a microduplex stainless steel by diffusion bonding using pure Cu as interlayer. In contrast, there is a steep hardness gradient in layer B, namely, in the vicinity of $Al_2O_3$, where the hardness reaches a maximum of 1261 $HV_{0.01}$. This drastic increase in hardness is consistent with the possible formation of oxide phases, resulting from the reaction between the ceramic sample and the molten brazing alloy.

The shear strength of joints at room temperature was $168 \pm 13$ MPa, which is about 50% of the shear strength of the base $Al_2O_3$ sample. A cross-section of the interface of the fractured joints after shear testing is presented in Fig. 4, showing that the fracture of joints occurred partially through the interface, mainly across layer B near the $Al_2O_3$ sample, and partially through the ceramic. It is worth noting that after shear testing, several cracks were then observed in layer B, denoting its brittleness. The cracks were observed close to the $Al_2O_3$ sample, where the interfacial hardness reaches the maximum value. Thus, the critical zone of the interface, regarding the mechanical strength of joints, is the hardest zone of layer B, which is probably composed of a mixture of $Ti_2$(Cu,Ni) intermetallics and oxide(s).

It is well established that the nature, morphology and properties of the reaction products formed at the interfaces are determinants of the overall properties of the joints. For instance, Shi et al. [23] used four different brazing temperatures (930 °C, 950 °C, 970 °C, and 990 °C) to join Zr-Si/Ti6Al4V using TiCuNi as filler. Results showed that the brazing temperature affected the microstructure of the brazed interfaces. The maximum shear strength (43 MPa) was achieved for brazing at 970 °C for 10 min. The authors stated that increasing the brazing temperature led to the increase of hypoeutectic and hypereutectic zones, which promoted the relief of the residual stresses in the joint. However, for the highest brazing temperature, in spite of the stress-relieving effect, the formation of coarse α-Ti adjacent to the Ti6Al4V was harmful to the shear strength of joints. Chang et al. [24] joined Ti6Al4V to Ti metal (15–3) alloys, using Ti-15Cu-15Ni and Ti-15Cu-25Ni as filler foils. Results showed that the presence of the Cu-Ni-rich phase was associated with lower shear strength and brittle fracture of the joints. He et al. [25] dopped Ti-15Cu-15Ni filler with rare-earth element Dy to understand its influence on the microstructure and mechanical properties of Ti6Al4V/Ti6Al4V joints. The authors concluded that by doping the filler with 0.05%wt. of Dy leads to the highest shear strength (777 MPa). The presence of a hard $Ti_2$(Ni, Cu) intermetallic layer in the brazing interface would be favourable for the improvement of the mechanical behaviour of the joint. Hong and Koo [18] join C103 and Ti6Al4V alloy by vacuum brazing using TiCuNi as filler. The authors investigated the influence of brazing temperature and holding time on the microstructure and shear strength of the joint. Joints brazed at 960 °C for 15 min presented the maximum shear strength (c.a. 360 MPa), and the authors related the mechanical behaviour of joints to the formation of a discontinuous zone composed of $Ti_2$(Cu,Ni) and/or $Ti_2$(Ni, Cu) intermetallics. On the other hand, the authors noticed that using the same brazing temperature but increasing the holding time from 15 to 20 min, the shear strength decreased to 298 MPa. This behaviour was attributed to the formation of a large amount of coarse acicular Widmanstätten structure at the interface. Wang et al. [26] brazed $Ti_2AlNb$ to Ti6Al4V using Ti-Zr-Cu-Ni filler with and without the incorporation of Mo. By incorporating 8% wt. of Mo, the shear strength

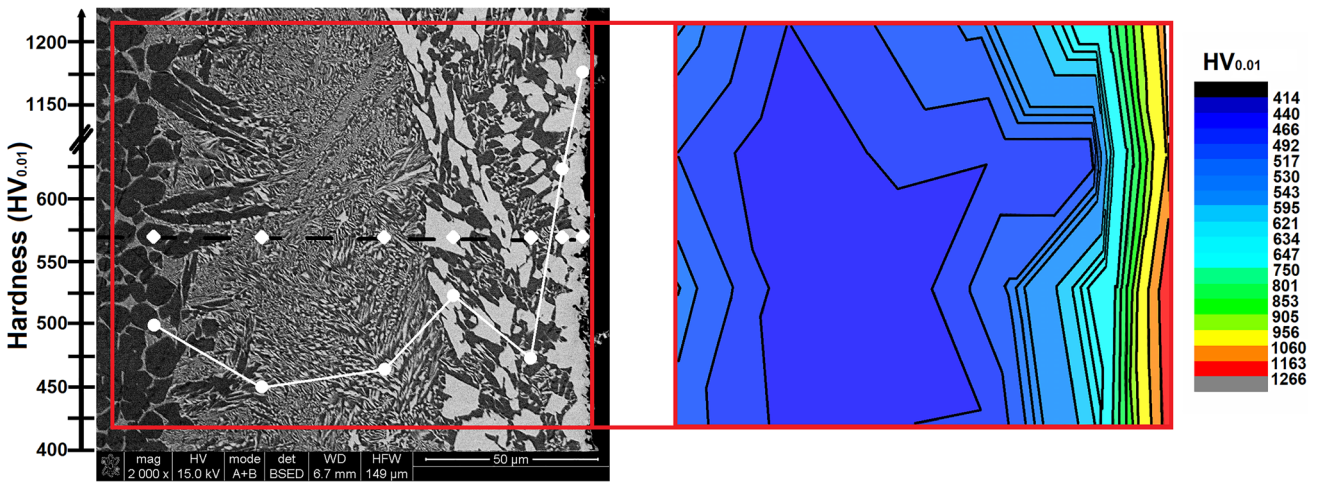


**Fig. 3** Interfacial hardness profile and interfacial hardness distribution map of joints

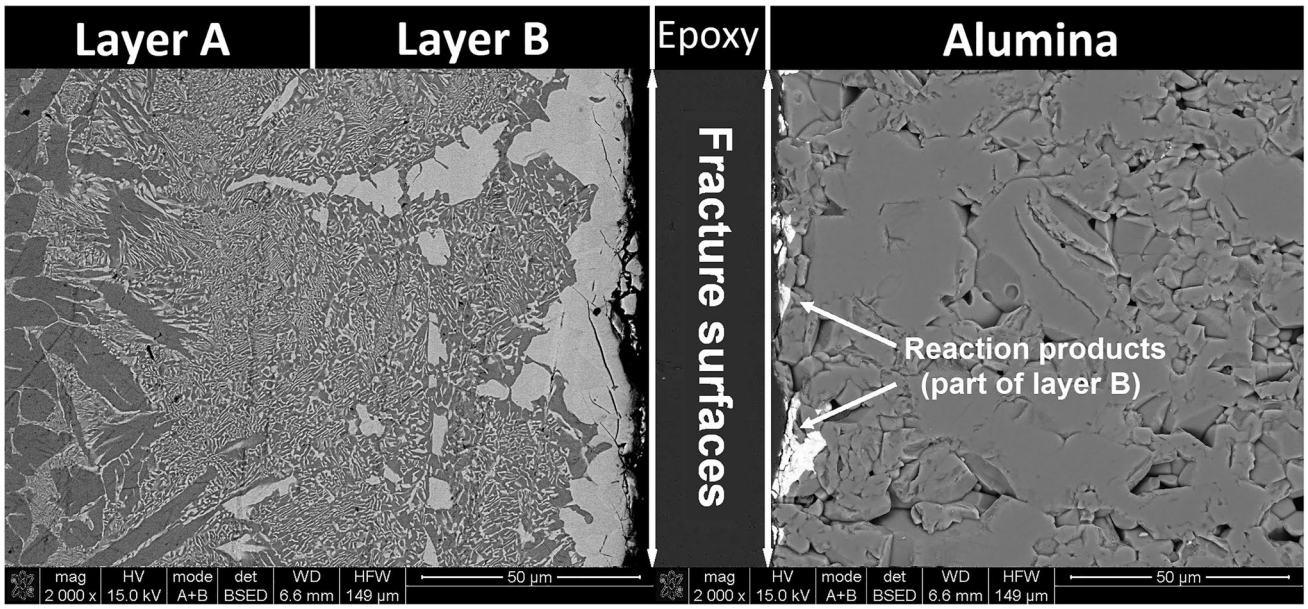


**Fig. 4** SEM images of the interface of fractured shear tested joints

increased up to 23%, when compared with the filler without the addition of Mo, reaching c.a. 350 MPa. The authors showed that the continuous $(Ti, Zr)_2(Cu, Ni)$ phase was the weakest part of the brazing joint.

The typical fracture surfaces of joints on the Ti6Al4V side and on the $Al_2O_3$ side of the interface are presented in Fig. 5.

After shear testing, the fracture surface on the Ti6Al4V side was completely covered by a thick black layer of reaction

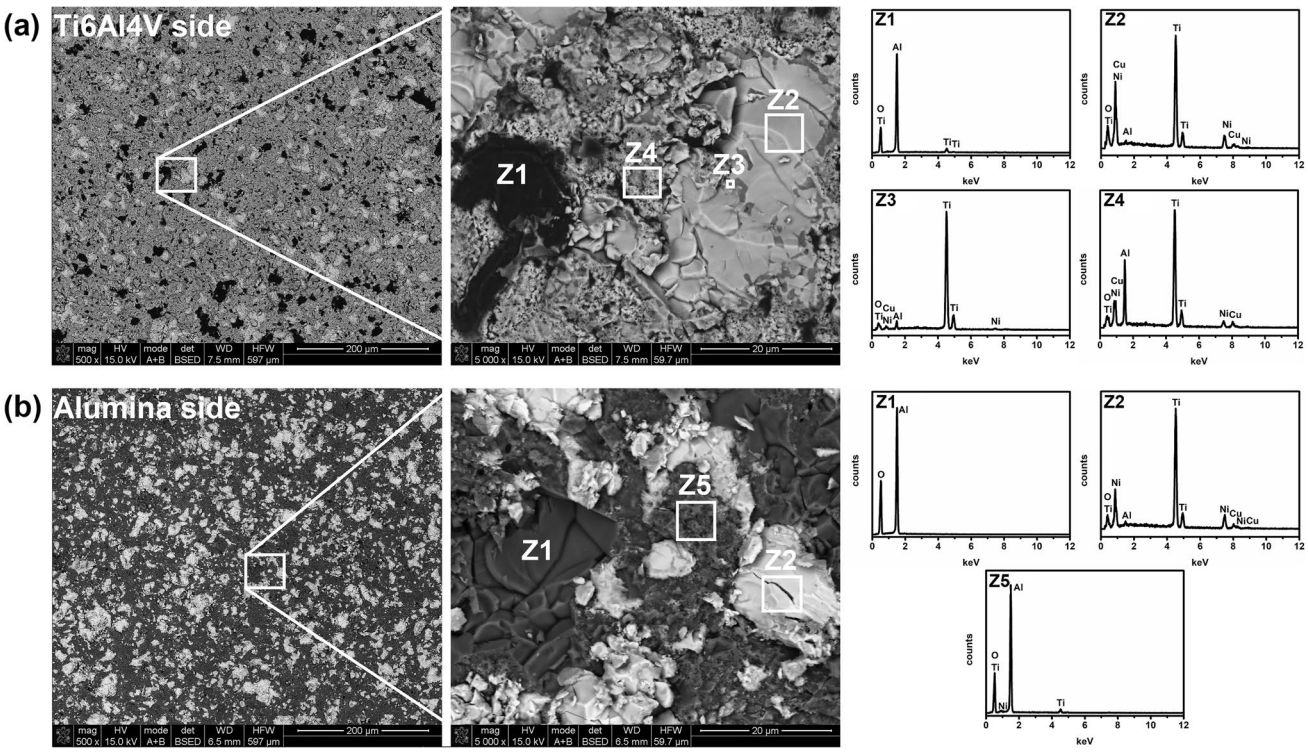


**Fig. 5** SEM images of the fracture surfaces of joints, showing a magnification of the indicated zones and the corresponding EDS spectra: (**a**) Ti6Al4V side and (**b**) alumina side

products, while the $Al_2O_3$ side was partially covered by a noticeably thinner one, and often, the ceramic broke into several pieces. On the Ti6Al4V side of the fracture surface, small dark pieces of $Al_2O_3$, labelled as Z1 in Fig. 5, were observed scattered throughout the entire surface. Zones presenting cleavage facets, labelled as Z2, were also detected on both fracture surfaces. According to their EDS spectra, these zones are essentially composed of Ti, Cu and Ni and thus should correspond to the $Ti_2$(Cu,Ni) intermetallic. The brittle nature of this intermetallic compound is in agreement with the observed typical cleavage facets. Zones labelled as Z3 are mainly composed of Ti and should be the α-Ti particles or eventually a Ti oxide since both may be present in layer B alongside with $Ti_2$(Cu,Ni) intermetallic. Noticeable rougher zones (Z4) with micro-voids, thus presenting ductile facture features, were also observed on the Ti6Al4V side of the fracture surface. These zones should correspond to the lamellar zones, predominantly composed of α-Ti, detected in layers A and B. Finally, on the $Al_2O_3$ side of the fracture surface, the EDS spectrum of dark grey zones, labelled as Z5, indicates the presence of Al, Ti and O. Considering both the EDS spectrum and the location of these zones, it is reasonable to admit that they should correspond to Ti oxide or mixed Ti–Al oxide in layer B near the $Al_2O_3$ sample. SEM images of the interface after shear testing and SEM images of the fracture surfaces show that fracture of joints occurred partially across the interface and partially across the $Al_2O_3$ sample. Facture across the interface occurred through layer B, predominantly near $Al_2O_3$, which is a quite brittle zone, denoted by the multiple cracks observed after shear testing, and by far the hardest zone of the interface. Some of the cracks that were nucleated in layer B near $Al_2O_3$ will be diverted towards the brittle ceramic sample, causing it to break partially into several fragments.

The XRD patterns of the fracture surface on the Ti6Al4V side are presented in Fig. 6 and indicate the detection α-Ti, β-Ti, $Ti_2Cu$, $Ti_2Ni$, $Ti_xO_y$ and $Al_2O_3$. It should be noted that the fracture surface on the Ti6Al4V side includes both base materials as well as the entire interface. The detection α-Ti, $Ti_2Cu$ and $Ti_2Ni$ is consistent with the formation of α-Ti and $Ti_2$(Cu, Ni) intermetallics at the interface. Additionally, $Ti_xO_y$ (in the form of $Ti_6O$, $(TiO_{1.27})_{0.787}$ and $TiO_{.176}$) was also detected. The detection of these $Ti_xO_y$ phases corroborates the formation of oxide phase(s) as interfacial reaction product(s), which should play a key role in the establishment of chemical bonding between the ceramic a metal phases. Finally, all of the phases composing the base materials, $Al_2O_3$ from the ceramic and α-Ti, β-Ti from Ti6Al4V, were also detected by XRD. Thus, combining the XRD results of the fracture surfaces, with SEM/EDS analysis results of the interface, allows us to describe the overall microstructural development across the joints as follows: base Ti6Al4V (α-Ti + β-Ti)/layer A: α-Ti + lamellar (α-Ti + $Ti_2$(Cu, Ni))/layer B: lamellar (α-Ti + $Ti_2$(Cu, Ni)) + $Ti_2$(Cu,Ni) + $Ti_xO_y$/base alumina ($Al_2O_3$).

Characteristic potentiodynamic polarisation curves of Ti6Al4V/TiCuNi/$Al_2O_3$ joints and Ti6Al4V (control group) are shown in Fig. 7a, and corrosion potential ($E_{(i=0)}$), passivation current density ($i_{pass}$) and galvanic potential ($E_{gal}$) values extracted from potentiodynamic polarisation curves are presented in Table 2. Considering the Ti6Al4V curve, it is possible to observe the typical potentiodynamic polarisation curve of a passive metal, where three distinct zones can be identified. Below the $E_{(i=0)}$, the current density is controlled by the

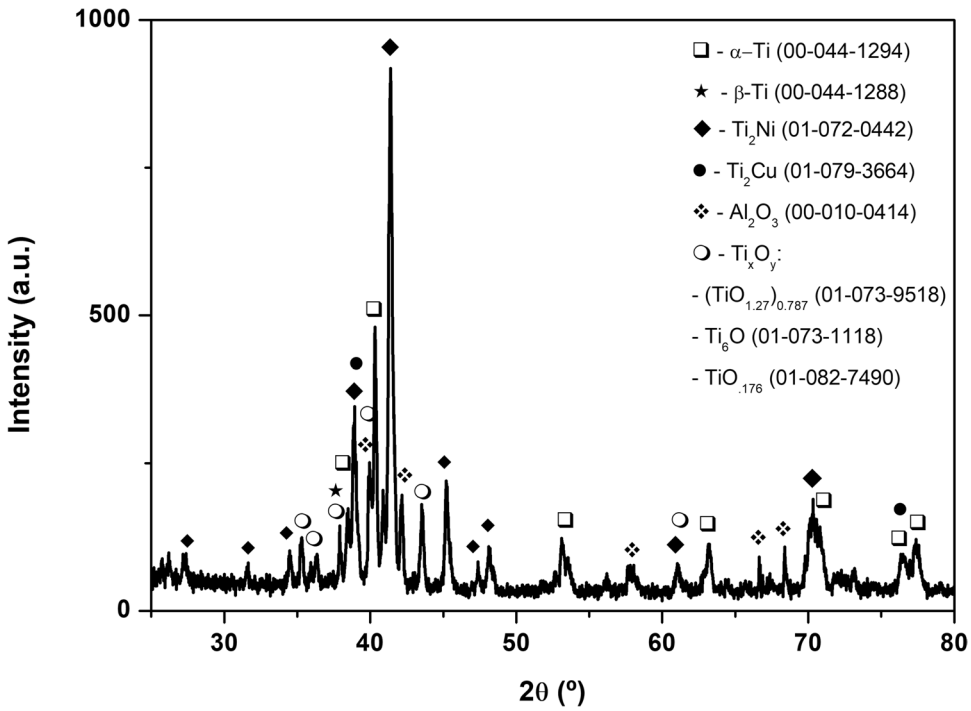


**Fig. 6** XRD patterns on the Ti6Al4V side of the fracture surface

reduction of water and dissolved oxygen, known as the cathodic domain. The region between the $E_{(i=0)}$ and $(0.101 \pm 0.016)$ $V_{Ag/AgCl}$ is called the active region. Just above the active zone, the passive domain starts, where the current density is constant as the potential values increase ($i_{pass}$). In this domain, the passive film formed is stable. On the other hand, for Ti6Al4V/TiCuNi/$Al_2O_3$ joints, a slow increase of the current densities on the anodic domain was observed, where could not be detected well-defined passivation plateau. However, this region can be denominated as a passivation region. Moreover, at c.a. 1.35 $V_{Ag/AgCl}$ ($E_{gal}$), the current density values suffered a sudden increase. When comparing both behaviours, it is possible to state that until approximately $E_{gal}$, both Ti6Al4V and Ti6Al4V/TiCuNi/$Al_2O_3$ joints presented a similar behaviour. These results show that until $E_{gal}$, no inferior electrochemical behaviour was observed for the brazed joints.

Chang and Chen [27] joined Ti6Al4V to Ti6Al4V using Ti-21Ni-14Cu as a brazing filler. The authors showed that the breakdown potential became nobler as the brazing time increased.

**Table 2** Corrosion potential ($E_{(i=0)}$), passivation current density ($i_{pass}$) and galvanic potential ($E_{gal}$) values of Ti6Al4V and brazed joints

| | $E_{(i=0)}$ ($V_{Ag/AgCl}$) | $i_{pass}^{*}$ ($\times 10^{-6}$ A $cm^{-2}$) | $E_{gal}$ ($V_{Ag/AgCl}$) |
|---|---|---|---|
| Ti6Al4V | $-0.35 \pm 0.03$ | $3.32 \pm 0.42$ | – |
| Ti64/TiCuNi/$Al_2O_3$ | $-0.28 \pm 0.04$ | $3.74 \pm 1.59$ | $1.35 \pm 0.10$ |

*$i_{pass}$ values were taken at 0.75 $V_{Ag/AgCl}$

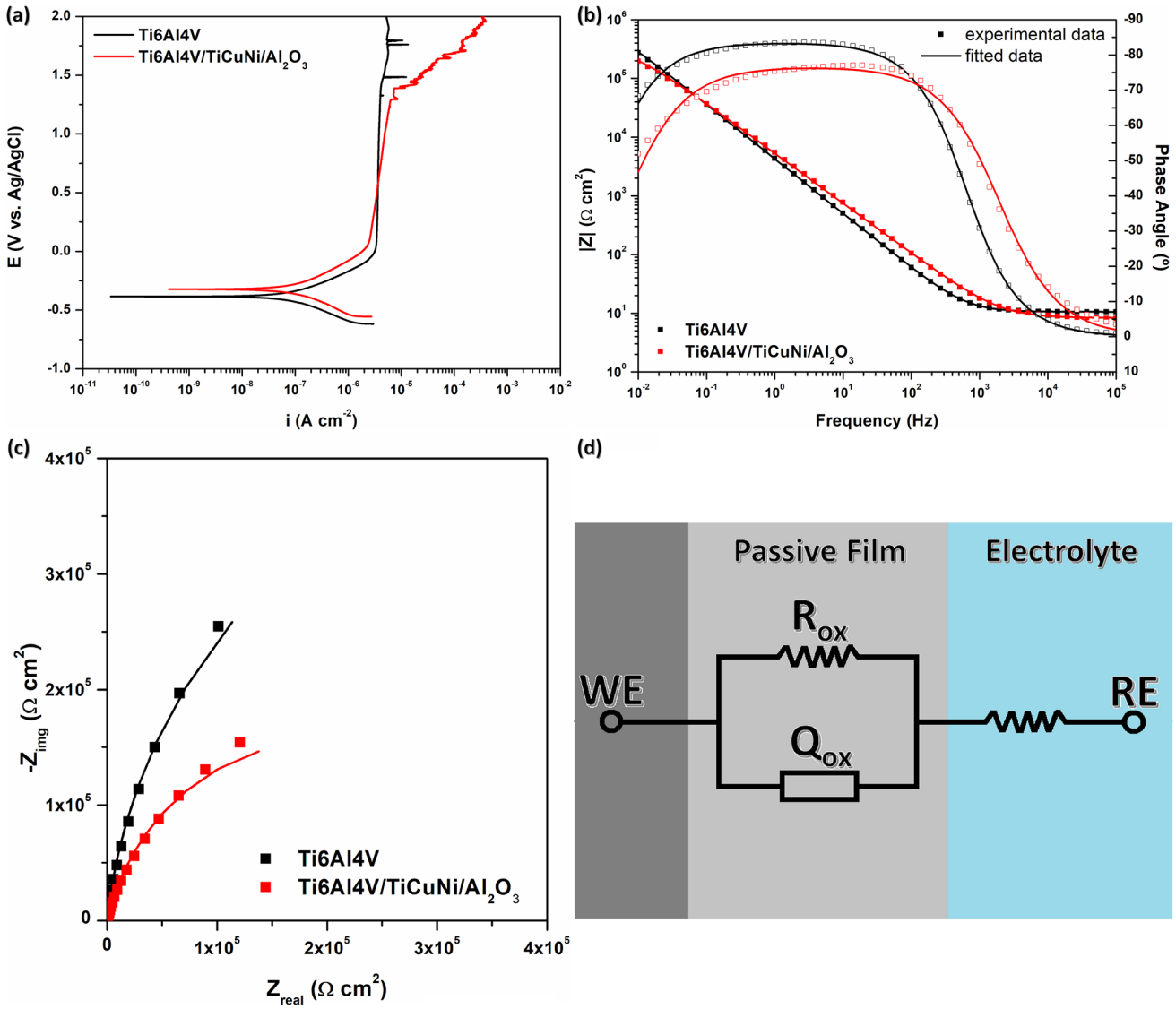


**Fig. 7** Corrosion behaviour of Ti6Al4V/TiCuNi/$Al_2O_3$ joints together with Ti6Al4V surfaces in 3.5% wt. NaCl: (**a**) representative potentiodynamic polarisation curves, EIS spectra in the form of (**b**) Bode and (**c**) Nyquist diagrams, and (**d**) EEC proposed

This behaviour was attributed to the decrease of intermetallic phase $Ti_2(Cu,Ni)$ or Cu and Ni atoms on the surface. Even though literature is limited on reporting the influence of intermetallic compounds on the corrosion behaviour of Ti-based alloys, generally, in terms of corrosion, the intermetallic phases are reported to be nobler than the metallic matrix. The formation of intermetallic compounds is reported to have an important responsibility on the corrosion behaviour of alloys. In fact, according to Osório et al. [28, 29], galvanic couples are formed between the intermetallics and α-phase lamellae. However, an "enveloping effect" between the intermetallics and α-phase was described, which minimises the galvanic effect, leading to better corrosion behaviour. Marinho et al. [13] investigated the effect of the filler material on the corrosion behaviour of similar Ti joints. The $Ti_2(Cu,Ni)$ intermetallics formed as the interface after brazing with TiCuNi filler did not jeopardise the corrosion behaviour of c.p. Ti. TiCuNi was also used to join Ti-$B_4C$ composites by Sousa et al. [14]. Results showed slightly that on the anodic domain, the recorded current densities were slightly lower in the case of the brazing interface on the anodic domain, which indicates a nobler corrosion behaviour than the base composite or the Ti-$B_4C$/TiCuNi/Ti-$B_4C$ joints. In both of these studies, the interfacial microstructure of the brazed joints was mainly composed of α-Ti and $Ti_2(Cu,Ni)$. However, the authors also reported some undissolved $B_4C$ reinforcement particles at the interface. In the present investigation, lamellar zones (α-Ti + $Ti_2(Cu,Ni)$) constitute most of the interface. However, as it can be observed in Fig. 2, $Ti_2(Cu,Ni)$ intermetallic is the main detected phase in layer B, especially in the vicinity of the $Al_2O_3$ sample. This might be the reason for the loss of passive behaviour. However, no evidence of galvanic corrosion was observed on the corroded surfaces shown in Fig. 8.

Representative Bode and Nyquist diagrams obtained from the Ti6Al4V and brazed joint are shown in Fig. 7b, c, respectively. In the Bode diagram, the constant values for |Z| in the high-frequency range ($10^3$ to $10^5$ Hz) together with a phase angle close to 0° are attributed to the electrolyte resistance. On the other hand, the phase angle presented values approaching −90° for low and middle frequencies for the base material and slightly lower on the brazed joints, which suggests the typical capacitive behaviour of a compact oxide film. Conversely, the total impedance of the system is taken from $|Z|_{f\to 0}$ corresponding to the corrosion resistance of the material, where the Ti6Al4V alloy presented slightly higher values when compared with brazed joints. On the other hand, the semicircle diameter represented in Nyquist diagrams shows the corrosion resistance; more particularly, higher corrosion resistance corresponds to higher semicircle diameter and therefore lower corrosion kinetics. As shown in Fig. 7c, the semicircle diameter of Ti6Al4V alloy was the highest, suggesting superior corrosion resistance, in agreement with the slightly higher values of $|Z|_{f\to 0}$ of the Bode diagram (Fig. 7b).

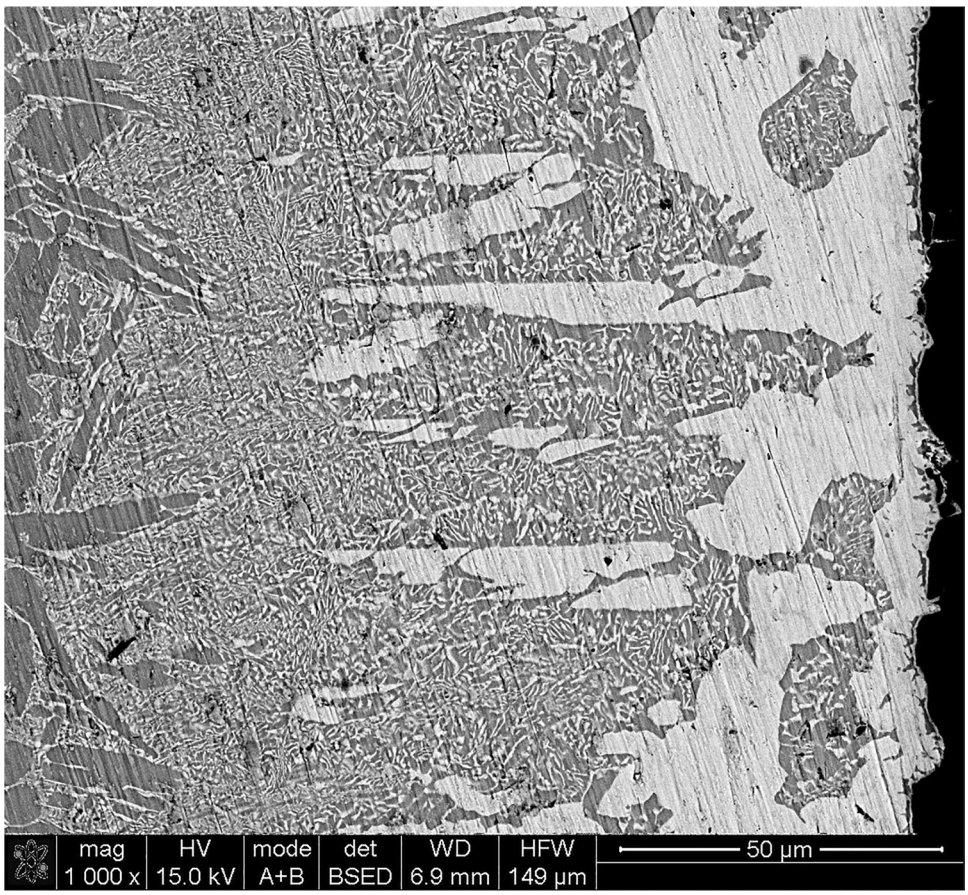


**Fig. 8** SEM image of corroded Ti6Al4V/TiCuNi/$Al_2O_3$ brazed joint (after potentiodynamic polarisation tests)

**Table 3** EIS parameters obtained by fitting with the proposed ECC

| | $R_e$ ($\Omega$ cm$^2$) | $R_{ox}$ ($\times 10^6$ $\Omega$ cm$^2$) | $Q_{ox}$ ($\times 10^{-5}$ S s$^a$cm$^{-2}$) | $n_{ox}$ | $\chi^2$ |
|---|---|---|---|---|---|
| Ti6Al4V | 10.43 ± 0.35 | 0.66 ± 0.26 | 4.47 ± 0.51 | 0.93 ± 0.01 | $< 10^{-3}$ |
| Ti6Al4V/TiCuNi/$Al_2O_3$ | 9.26 ± 2.32 | 0.63 ± 0.55 | 3.64 ± 1.59 | 0.85 ± 0.01 | $< 10^{-3}$ |

Figure 7d presents the EEC for the passive film formed on Ti6Al4V and brazed joints used in the fitting of the experimental data, containing $R_e$ – resistance of the electrolyte and $R_{ox}/Q_{ox}$ pair consisting of the passive film resistance and constant phase element (CPE), respectively. Considering the non-ideal capacitance behaviour of the passive film, a CPE was used. The EEC parameters obtained from EIS data for the Ti6Al4V and brazed joints are shown in Table 3. The impedance of a CPE is given as $Z_{CPE} = \left[Y_0(j\omega)^n\right]^{-1}$, where $Y_0$ is CPE admittance in $\Omega^{-1}s^n cm^{-2}$, $j = \sqrt{-1}$ is the imaginary unit, $\omega = 2\pi f$ is the angular frequency in $rad/s$, and $n$ is dimensionless number. If $n = -1$, $n = 0$ or $n = 1$ the CPE represents an inductor, resistor and capacitor, respectively. Moreover, $n$ values are between $-1$and1. The $n$ value c.a. 1 represents the non-ideal capacitor behaviour by CPE being influenced by the surface roughness and heterogeneities, which leads to a non-uniform current distribution.

As it can be seen in Table 3, the $R_{ox}$ on Ti6Al4V is slightly higher than the one formed on the brazed joints. On the other hand, $Q_{ox}$ values of the brazed joint are slightly lower than in the case of Ti6Al4V. However, $n$ values of the brazed joints are lower than for Ti6Al4V. EIS results are in agreement with the potentiodynamic polarisation parameters. Also, the standard deviation for brazed joints is always higher when compared with Ti6Al4V, which might be linked to the evolution of the interfacial microstructure from the metal to the ceramic in the joints. There are only a few studies focussing on the electrochemical behaviour of the brazed joints, and characterisation through the EIS technique is even scarcer. To the best of the author's knowledge, just three studies reported the EIS behaviour of joined materials [14, 30, 31]. Avila and Rocha [31] used EIS measurements to access the corrosion resistance of Ti/glass–ceramic interfaces obtained by active metal brazing. EIS results allowed us to identify that the galvanic interactions occurred mainly between the Cu and the Ag-rich layers. On the other hand, Lee MK and Lee JG [30] confirmed by EIS that the segregated intermetallic phase, as its resistance to galvanic corrosion was lower when compared to the Ti–rich phase around either its vicinal region or the Ti6Al4V base metal, presented the higher corrosion resistance. Finally, Sousa et al. [14] identified the different responses of the Ti matrix and the $Ti_2$(Cu,Ni) intermetallics formed at the brazed interface. The EEC used by the authors described a pair $R_{Ti}/Q_{Ti}$ representing the resistance and capacitance of the Ti matrix; moreover, the authors added a second pair $R_{int}/Q_{int}$ corresponding to the resistance and capacitance of the intermetallic compounds formed at the brazed interface. Results showed that the intermetallic compounds presented higher corrosion resistance and as well slightly lower Q values, showing the better quality of the film formed on the intermetallic surfaces.

The evolution of OCP and $R_p$ with the immersion period is presented in Fig. 9. $R_p$ parameter was deduced by linear polarisation curves. In both cases, the OCP values increased through

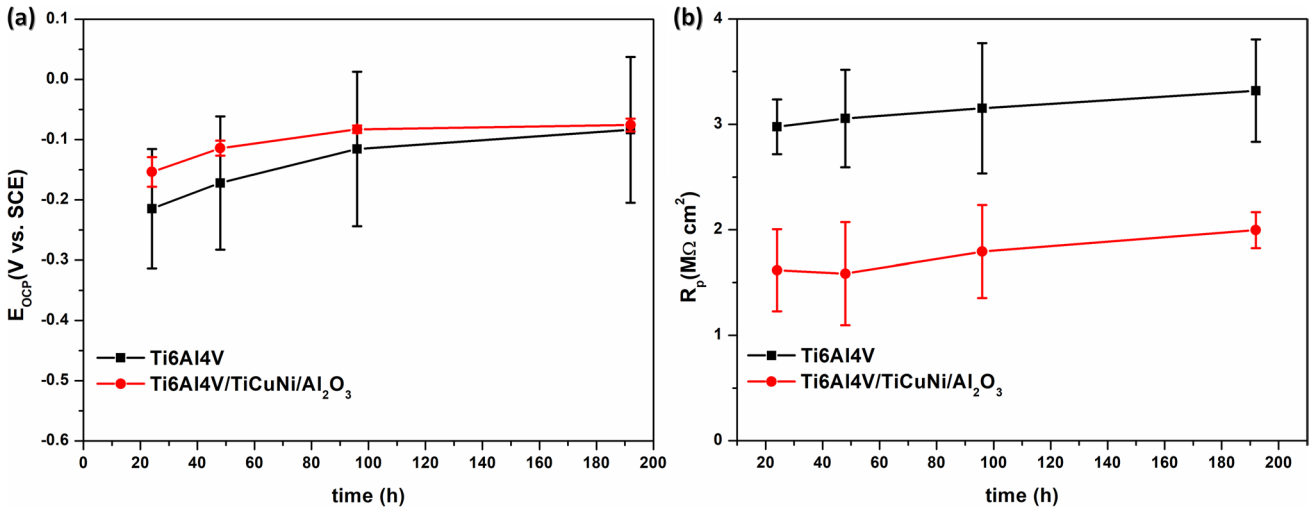


**Fig. 9** Evolution of (**a**) open circuit potential ($E_{OCP}$) and (**b**) polarisation resistance ($R_p$) with the immersion time

the immersion period, showing the ability of the brazed joints to form a protective film that leads to a decrease in the susceptibility to corrosion as the immersion time increased. For the first days of immersion, brazed joints presented slightly nobler OCP values than the Ti6Al4V base material. Instead, $R_p$ values also increased through the immersion period. However, brazed joints showed lower values when compared to Ti6Al4V, which indicates higher corrosion kinetics. This behaviour might be explained by the differences between the exposed areas of the intermetallic phases and of Ti6Al4V, together with a mixed effect related to the differences between the individual microstructural features and chemical compositions of the phases formed at the brazing interface.

## 4 Conclusions

The effect TiCuNi brazing filler on of the mechanical and corrosion behaviour of Ti6Al4V/$Al_2O_3$ joints was studied. The results obtained in this investigation allowed the following conclusions to be drawn.

- Brazing Ti6Al4V to $Al_2O_3$ using TiCuNi filler alloy at 980 °C produced a sound-layered interface.
- No noticeable alterations in the microstructure or the chemical composition of both base materials were induced by the joining process.
- The microstructure of the brazed joint could be summarised as follows: base Ti6Al4V (α-Ti + β-Ti)/layer A: α-Ti + lamellar (α-Ti + $Ti_2$(Cu, Ni))/layer B: lamellar (α-Ti + $Ti_2$(Cu, Ni)) + $Ti_2$(Cu,Ni) + $Ti_xO_y$/base alumina ($Al_2O_3$), where $Ti_xO_y$ stands for $Ti_6O$, $(TiO_{1.27})_{0.787}$ and $TiO_{.176}$.
- The interface is harder than the base Ti6Al4V alloy and tends to increase from layer A (between around 450 and 500 $HV_{0.01}$) towards the ceramic sample, reaching the maximum of 1261 $HV_{0.01}$ in the vicinity of the $Al_2O_3$ sample, where the interface consists essentially in a mixture of $Ti_2$(Cu,Ni) intermetallics and $Ti_xO_y$.
- The shear strength of joints was 168 ± 13 MPa, and fracture occurred partially through the hardest zone of the interface and partially through the ceramic sample.
- The phases constituting the interface did not have a noticeable impact on the corrosion behaviour of joints when compared to Ti6Al4V.

**Funding** This work was supported by the Portuguese Foundation for Science and Technology (FCT), Portugal, under PTDC/CTM-CTM/31579/2017—POCI-01–0145-FEDER – 031579 – funded by FEDER funds through COMPETE2020—Programa Operacional Competitividade e Internacionalização (POCI) and by national funds (PIDDAC) through FCT/MCTES.

**Data availability** The authors confirm that the data supporting the findings of this study are available within the article.

## Declarations

**Conflict of interest** The authors declare no competing interests.

## References

1. Peng Y, Li J, Shi J et al (2021) Microstructure and mechanical properties of $Al_2O_3$ ceramic and $Ti_2AlNb$ alloy joints brazed with $Al_2O_3$ particles reinforced Ag–Cu filler metal. Vacuum 192:110430. https://doi.org/10.1016/j.vacuum.2021.110430
2. Qiu Q, Wang Y, Yang Z, Wang D (2016) Microstructure and mechanical properties of $Al_2O_3$ ceramic and Ti6Al4V alloy joint brazed with inactive Ag-Cu and Ag-Cu + B. J Eur Ceram Soc 36:2067–2074. https://doi.org/10.1016/j.jeurceramsoc.2016.02.033
3. Liu Z, He B, Lyu T, Zou Y (2021) A review on additive manufacturing of titanium alloys for aerospace applications: directed energy deposition and beyond Ti-6Al-4V. Jom 73:1804–1818. https://doi.org/10.1007/s11837-021-04670-6
4. Jha AK, Singh SK, Swathi Kiranmayee M et al (2010) Failure analysis of titanium alloy (Ti6Al4V) fastener used in aerospace application. Eng Fail Anal 17:1457–1465. https://doi.org/10.1016/j.engfailanal.2010.05.007
5. Yi J, Zhang Y, Wang X et al (2016) Characterization of Al/Ti nano multilayer as a jointing material at the interface between Cu and $Al_2O_3$. Mater Trans 57:1494–1497. https://doi.org/10.2320/matertrans.M2016126
6. Kozlova O, Braccini M, Voytovych R et al (2010) Brazing copper to alumina using reactive CuAgTi alloys. Acta Mater 58:1252–1260. https://doi.org/10.1016/j.actamat.2009.10.029
7. Asthana R, Singh M (2008) Joining of partially sintered alumina to alumina, titanium, Hastealloy and C-SiC composite using Ag-Cu brazes. J Eur Ceram Soc 28:617–631. https://doi.org/10.1016/j.jeurceramsoc.2007.06.017
8. Jing Y, Yue X, Gao X et al (2016) The influence of Zr content on the performance of TiZrCuNi brazing filler. Mater Sci Eng A 678:190–196. https://doi.org/10.1016/j.msea.2016.09.115
9. Elrefaey A, Tillmann W (2009) Effect of brazing parameters on microstructure and mechanical properties of titanium joints. J Mater Process Technol 209:4842–4849. https://doi.org/10.1016/j.jmatprotec.2009.01.006
10. Chang CT, Shiue RK (2005) Infrared brazing Ti-6Al-4V and Mo using the Ti-15Cu-15Ni braze alloy. Int J Refract Met Hard Mater 23:161–170. https://doi.org/10.1016/j.ijrmhm.2005.01.002
11. Singh M, Shpargel TP, Morscher GN, Asthana R (2005) Active metal brazing and characterization of brazed joints in titanium to carbon-carbon composites. Mater Sci Eng A 412:123–128. https://doi.org/10.1016/j.msea.2005.08.179
12. Hardesty R, Jensen M, Grant L (1989) High temperature be panel development. NASA Contract Report 181777. Electrofusion Corporation, Fremont
13. Marinho C, Toptan F, Guedes A, Alves AC (2021) Electrochemical response of Ti joints vacuum brazed with TiCuNi, AgCu, and Ag fillers. Trans Nonferrous Met Soc China 31:999–1011. https://doi.org/10.1016/S1003-6326(21)65556-5
14. Sousa JM, Alves AC, Toptan F et al (2019) Corrosion and tribocorrosion behavior of Ti-B4C composites joined with TiCuNi brazing alloy. J Mater Eng Perform 28:4972–4982
15. Villars P (1994) Handbook of ternary alloy phase diagrams. ASM International

16. Lee SJ, Wu SK, Lin RY (1998) Infrared joining of TiAl intermetallics using Ti-15Cu-15Ni foil-I. The microstructure morphologies of joint interface. Acta Mater 46:1283–1295
17. Lee SJ, Wu SK, Lin RY (1998) Infrared joining of TiAl intermetallics using Ti-15Cu-15Ni foil - II. The microstructural evolution at high temperature. Acta Mater 46:1297–1305
18. Hong I-T, Koo C-H (2005) Vacuum-furnace brazing of C103 and Ti–6Al–4V with Ti–15Cu–15Ni filler-metal. Mater Sci Eng A 398:113–127. https://doi.org/10.1016/j.msea.2005.03.007
19. Hong IT, Koo CH (2005) The study of vacuum-furnace brazing of C103 and Ti-6Al-4V using Ti-15Cu-15Ni foil. Mater Chem Phys 94:131–140. https://doi.org/10.1016/j.matchemphys.2005.04.021
20. Gomes L, Guedes A (2016) Influence of the Brazing filler on the microstructure of Ti6Al4V joints. Microsc Microanal 22:40–41. https://doi.org/10.1017/S1431927616000398
21. Liu XP, Zhang LX, Sun Z, Feng JC (2018) Microstructure and mechanical properties of transparent alumina and TiAl alloy joints brazed using Ag-Cu-Ti filler metal. Vacuum 151:80–89. https://doi.org/10.1016/j.vacuum.2018.01.019
22. Eroğlu M, Khan TI, Orhan N (2002) Diffusion bonding between Ti-6Al-4V alloy and microduplex stainless steel with copper interlayer. Mater Sci Technol 18:68–72. https://doi.org/10.1179/026708301125000230
23. Shi JM, Zhang LX, Pan XY et al (2018) Microstructure evolution and mechanical property of ZrC-SiC/Ti6Al4V joints brazed using Ti-15Cu-15Ni filler. J Eur Ceram Soc 38:1237–1245. https://doi.org/10.1016/j.jeurceramsoc.2017.11.045
24. Chang CT, Du YC, Shiue RK, Chang CS (2006) Infrared brazing of high-strength titanium alloys by Ti-15Cu-15Ni and Ti-15Cu-25Ni filler foils. Mater Sci Eng A 420:155–164. https://doi.org/10.1016/j.msea.2006.01.046
25. He Y, Lu C, Ni C et al (2020) Tailoring microstructure and mechanical performance of the TC4 titanium alloy brazed joint through doping rare-earth element Dy into Ti-Cu-Ni filler alloy. J Manuf Process 50:255–265. https://doi.org/10.1016/j.jmapro.2019.12.044
26. Wang Y, Jiao M, Yang Z et al (2018) Vacuum brazing of Ti2AlNb and TC4 alloys using Ti–Zr–Cu–Ni and Ti–Zr–Cu–Ni + Mo filler metals: microstructural evolution and mechanical properties. Arch Civ Mech Eng 18:546–556. https://doi.org/10.1016/j.acme.2017.10.006
27. Chang E, Chen CH (1997) Low-melting-point titanium-base brazing alloys-part 2: characteristics of brazing Ti-21Ni-14Cu on Ti-6Al-4V substrate. J Mater Eng Perform 6:797–803. https://doi.org/10.1007/s11665-997-0084-2
28. Osório WR, Cremasco A, Andrade PN et al (2010) Electrochemical behavior of centrifuged cast and heat treated Ti-Cu alloys for medical applications. Electrochim Acta 55:759–770. https://doi.org/10.1016/j.electacta.2009.09.016
29. Osório WR, Freire CM, Caram R, Garcia A (2012) The role of Cu-based intermetallics on the pitting corrosion behavior of Sn-Cu, Ti-Cu and Al-Cu alloys. Electrochim Acta 77:189–197. https://doi.org/10.1016/j.electacta.2012.05.106
30. Lee MK, Lee JG (2013) Mechanical and corrosion properties of Ti-6Al-4V alloy joints brazed with a low-melting-point 62.7Zr-11.0Ti-13.2Cu-9.8Ni-3.3Be amorphous filler metal. Mater Charact 81:19–27
31. Avila EA, Rocha LA (2005) Evaluation of corrosion resistance of multi-layered Ti/glass-ceramic interfaces by electrochemical impedance spectroscopy. Mater Sci Forum 492–493:189–194. https://doi.org/10.4028/www.scientific.net/msf.492-493.189